Hindawi
International Journal of Optics
Volume 2019, Article ID 2032870, 12 pages
https://doi.org/10.1155/2019/2032870

*Research Article*

# Progressive Multifocal Liquid Lenses Based on Asymmetric Freeform Surface Structure of Nonuniform Thickness Elastic Membranes with Different Constraints

**Weiliang Jia, Biao Zhang, and Songjing Li**

*Department of Fluid Control and Automation, Harbin Institute of Technology, 2 Yikuang Street, Harbin 150001, China*

Correspondence should be addressed to Biao Zhang; zhangbiao@hit.edu.cn and Songjing Li; lisongjing@hit.edu.cn

Received 17 July 2019; Revised 1 September 2019; Accepted 20 September 2019; Published 27 October 2019

Academic Editor: Giancarlo C. Righini

Copyright © 2019 Weiliang Jia et al. This is an open access article distributed under the Creative Commons Attribution License, which permits unrestricted use, distribution, and reproduction in any medium, provided the original work is properly cited.

For a progressive multifocal liquid lens with an elastic membrane deformed by liquid pressure, to realize a reasonably power distribution, asymmetric deformation characteristics of the membrane surface are needed. Based on the asymmetric freeform surface structure, this paper proposed progressive multifocal liquid lenses focused by liquid with nonuniform thickness membranes. The structure and mathematical model of power distribution for the lens are introduced. The membrane deformation and the corresponding power distribution of the lenses with asymmetric freeform surface are predicted and compared under uniform pressure load and different boundary conditions using the finite element method. An optical testing system is constructed to analyze the optical characteristics of the fabricated lenses through observing the focusing performance of the F target image at different regions of the lenses. Experimental results show that the liquid lenses can realize as asymmetrical progressive multifocal liquid lenses after liquid accommodation; meanwhile, the trends of power distribution of the lenses generally agree well with simulations.

## 1. Introduction

Focus-tunable liquid lenses have attracted a great deal of attention in recent years, which can change the optical power distribution more smoothly by modifying the amount of liquid through tuning the internal liquid pressure of the lens [1–4]. Traditionally, a liquid lens is composed of a chamber with one side being a thin elastic membrane and the other being a transparent window; moreover, finite element method (FEM) is usually applied to simulate the membrane deformation under different boundary conditions and loading [4–8]. Focus-tunable liquid micro lenses with elastic membranes were also developed and analyzed through controlling actuators to adjust the pressure of liquid and alter the radius of curvature of the membrane [9, 10]. Likewise, a liquid plano-convex mini lens with focal length tunable is constructed and the focal length of the lens can be adjusted through changing the amount of oil droplet or adding an external force onto the lens [11]. Furthermore, a varifocal liquid lens actuated by laser-induced thermal Marangoni forces is introduced which changes a local curvature of the droplet surface due to the thermocapillary displacement of liquid droplet caused by heating with a laser beam [12].

In addition, tunable focus liquid lenses with large optical aperture were also introduced, which provided larger range of tunable power [13–16]. In order to reduce gravity effects to the performance of liquid lens, one method used an in-plane pretention force onto the membrane to take the place of surface tension and another used a nonuniform thickness profile of flexible membrane [17, 18]. Furthermore, the focus-tunable liquid lenses using nonuniform thickness membranes are also introduced and have some advantages compared with the lens with a uniform thickness membrane of alleviating the edge clamping effect, reducing spherical aberration and improving optical resolutions [19–23].

The liquid lenses introduced above have one focus, and the focus only can be tuned along an axis. In this study,

progressive multifocal liquid lenses are proposed which have two focuses, and they can be adjusted simultaneously using the deformation characteristics of nonuniform thickness membranes with different constraints. The desired surface shape of nonuniform thickness membrane after deformation should be an aspherical surface; meanwhile, the type of constraint is the key to obtain a progressive multifocal liquid lens. Moreover, the surface of membrane after deformation can be considered as a freeform surface structure with different constraint conditions. In the field of architecture, there was a freeform surface structure which defined specified fixed points of the perimeter as the geometric constraint conditions [24]. In addition, NURBS (nonuniform rational B-spline) is an effective method to express the geometry of freeform shell structures through the coordinates of the NURBS control points, and restressed membrane roofs of freeform could be suspended on arches or suspension cables [25, 26]. From above, we can draw from the form of constraint conditions of freeform surface structures in the field of architecture to obtain desired asymmetric membrane in the design of multifocal liquid lens.

Based on the design of freeform surface structures with kinds of constraint conditions, in this study, progressive multifocal liquid lenses are proposed by considering the deformation characteristics of nonuniform thickness membranes and corresponding optical power distribution. Several elastic membranes of 3D models of nonuniform thickness are built in the software of SolidWorks, and then the corresponding deformation is calculated by using FEM simulations under different boundary conditions and uniform pressure load. Subsequently, three kinds of progressive multifocal liquid lenses are designed based on the deformation characteristics of the nonuniform thickness membranes, and an optical testing system is built to analyze the focusing performance of the proposed lenses. The potential applications of the proposed progressive multifocal liquid lens can be in the field of tunable optics and in the field of vision correction especially for the old people who can change the power value at different environments.

## 2. Structure and Mathematical Model of Optical Power Distribution for the Lens

Tunable liquid lenses with a uniform thickness membrane or a nonuniform thickness membrane are shown in Figure 1, which mainly consist of an elastic membrane, a substrate, constraint, liquid chamber, and a pinhole. For the liquid lens with uniform thickness membrane whose thickness is $t$, the membrane deforms and rotates symmetrically with respect to the optical axis under uniform pressure load and circular constraint; however, for the liquid lens with nonuniform thickness membrane whose thickness changes from $t_1$ to $t_2$, the membrane deforms and rotationally asymmetric. The coordinates of ($x$, $y$, $z$) for the liquid lens are shown in Figure 1(c), and the coordinate of $z$ is the direction of the surface membrane to deform.

In this study, polydimethylsiloxane (PDMS) is used as the material of elastic membrane because of its good optical transparency (≥95%), long elongation, and ease of fabrication process. The material chosen for the substrate of liquid lens is polymethylmethacrylate (PMMA) (refractive index $n = 1.49$) because of high transparency (≥92%) and good mechanical properties. Furthermore, the deionized water is used as the liquid ($n = 1.33$) which is pumped into the chamber of the lens through the pinhole by means of an external syringe pump, and then the membrane deformed depending on the liquid pressure leading to the change of the curvature of the membrane surface. In addition, the constraint is not only a connecting device between the membrane and substrate but also an edge-clamped device of the liquid lens.

The optical power distribution is the main evaluation index of a progressive multifocal liquid lens, which is expressed as spherical power $D$, and the corresponding contour plots can be calculated through the following equation [27, 28]:

$$D = 1000\,(n-1)\frac{k_1 + k_2}{2} = 1000\,(n-1)H, \tag{1}$$

where $H$ is the mean curvature of one point of the lens surface, $n$ is the refractive index of the lens, and $k_1$ and $k_2$ are the orthogonal curvature of any point on the lens surface, which satisfy the quadratic equations as follows:

$$g^4k^2 + g\left[2pqs - \left(1+p^2\right)t - \left(1+q^2\right)r\right]k + \left(rt - s^2\right) = 0, \tag{2}$$

where $p = (\partial z/\partial x)$, $q = (\partial z/\partial y)$, $r = (\partial^2 z/\partial x^2)$, $s = (\partial^2 z/\partial x\,\partial y)$, $t = (\partial^2 z/\partial y^2)$, and $g = \sqrt{1 + p^2 + q^2}$.

The value of the surface vector heights of a lens can be described by the equation $z = f(x, y)$, where $x$, $y$, and $z$ are rectangular Cartesian coordinates, and $p$, $q$, $r$, $s$, and $t$ are the differentials of all kinds of order of surface sag. By solving the equation (2), the mean curvature can be expressed as

$$H = \frac{k_1 + k_2}{2} = \frac{\left(1+p^2\right)t + \left(1+q^2\right)r - 2pqs}{2g^3}. \tag{3}$$

In this study, several 3D models of nonuniform thickness elastic membranes are constructed in the software of SolidWorks and inputted into the software of Ansys, and then the deformation data onto the membranes under uniform surface pressure load can be obtained through FEM simulation with different boundary conditions; therefore, the optical power distribution can be calculated and evaluated through equations above.

## 3. Predicted Deformation Characteristics of the Nonuniform Freeform Surface Membrane and Optical Power Distribution of the Lens

The software of ANSYS can be used to do FEM simulation, in this study, ANSYS is employed to obtain the deformation characteristics of PDMS membranes under different boundary conditions. Firstly, the models of 3D geometry of membranes in the software of SolidWorks are established, and then the models are transferred to ANSYS for meshing and simulation. The parameters of PDMS membrane of

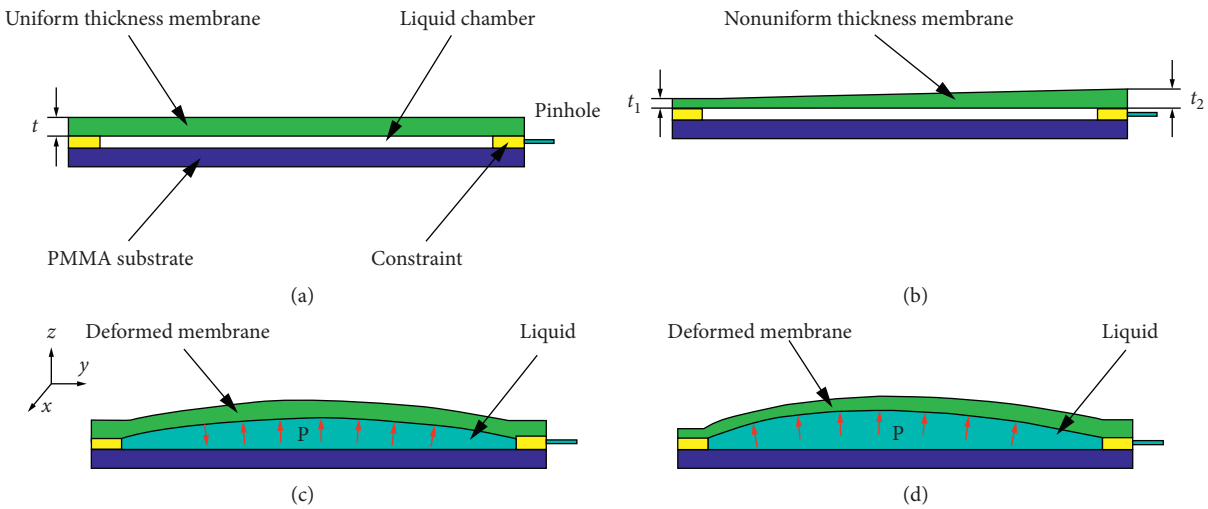


Figure 1: Schematic depiction of tunable liquid lenses. (a) Lens with a uniform thickness membrane before liquid injection. (b) Lens with a nonuniform thickness membrane before liquid injection. (c) Lens with uniform thickness deformed membrane after liquid injection. (d) Lens with a nonuniform thickness deformed membrane after liquid injection.

Young's modulus, Poisson's ratio, and density are set as 1.2 MPa, 0.46, and 982 kg/m$^3$, respectively [4]. Then, the parameters are input into ANSYS, and the meshed type, boundary conditions, and load pressure are set; after the simulation, the raw data onto the deformed profile is generated. Finally, the digital data onto the membrane deformation are analyzed with Microsoft Excel program and then transferred into the software of MATLAB to calculate the optical power distribution through equations (1) and (2). The most important is that the design rule of liquid lenses is to obtain a power value of +4$D$/+6$D$ in the far/near vision region, and the optimization approach is to adjust the thickness distribution for circular membranes and try different constraints between elastic membrane and support plate under uniform surface pressure.

*3.1. Characteristics of the Deformation and Optical Power Distribution for Nonuniform Membranes with Full Edge Clamped.* Two kinds of structures of 3D geometry of circular membranes are designed and simulated with full edge clamped of boundary condition as shown in Figure 2. Figure 2(a) shows the front view of circular membranes and the diameter is 30 mm, Figures 2(b) and 2(c) show the side view of two kinds of structures of 3D geometry of circular membranes, and the numbers are in millimeters. Also, the coordinates of ($x$, $y$, $z$) for the membrane are shown in Figure 2(a) with the coordinate of $z$ is the direction of the membrane to deform. Then, the thickness distribution of the two shapes of membranes are one direction inclined and two directions inclined as shown in Figures 2(b) and 2(c). In addition, the freeform surface structure of the circular membrane after deformation with constraint of full edge clamped is predicted as shown in Figure 2(d).

Then, two geometry models of Figures 2(b) and 2(c) are transferred to ANSYS software for meshing and simulation with the constraint of full edge clamped, and the deformation displacement contour maps of membranes with front view and left view under pressures of 106 Pa and 167 Pa are shown in Figures 3(a) and 3(b).

Furthermore, the digital data of deformation displacement of membranes are analyzed with Microsoft Excel program and then inputted into the software of MATLAB to calculate the surface mean power according to equations (1) and (2), as illustrated in Figures 3(c) and 3(d). The aim of the simulation is to attain a progressive multifocal lens with a power distribution of +4$D$ ($f$ = 250 mm) at the far view region and +6$D$ ($f$ = 167 mm) at the near view region. For the model with one direction inclined as shown in Figure 2(b), the optical power distribution changes from +4$D$ to +6$D$ obtained under the pressure of 106 Pa as shown in Figure 3(c), while for the model with two directions inclined as shown in Figure 2(c), it has two focuses and its corresponding power are +4.03$D$ in the far view point and +5.99$D$ in the near view point as shown in Figure 3(d). That is, only the model with two directions inclined with constraint of full edge clamped can obtain multifocal under uniform pressure onto the surface of the membrane.

*3.2. Characteristics of the Deformation and Optical Power Distribution for Nonuniform Membranes with Part of Edge Clamped.* For the liquid lens of PDMS membrane with part of edge clamped, the liquid-filled cavity of the lens is sealed with a piece of uniform thickness PDMS membrane and a piece of nonuniform thickness PDMS membrane which can be designed, and then adhesive films located at the edge of the lens can be used as the constraint to bond PDMS membrane together with a PMMA plate. So, another two kinds of nonuniform thickness membranes are designed; one of them is a circular membrane with double directions incline with constraint of two parts of edge clamped, and its front view and side view are shown in Figures 4(a) and 4(b). The other is a nonuniform thickness membrane with

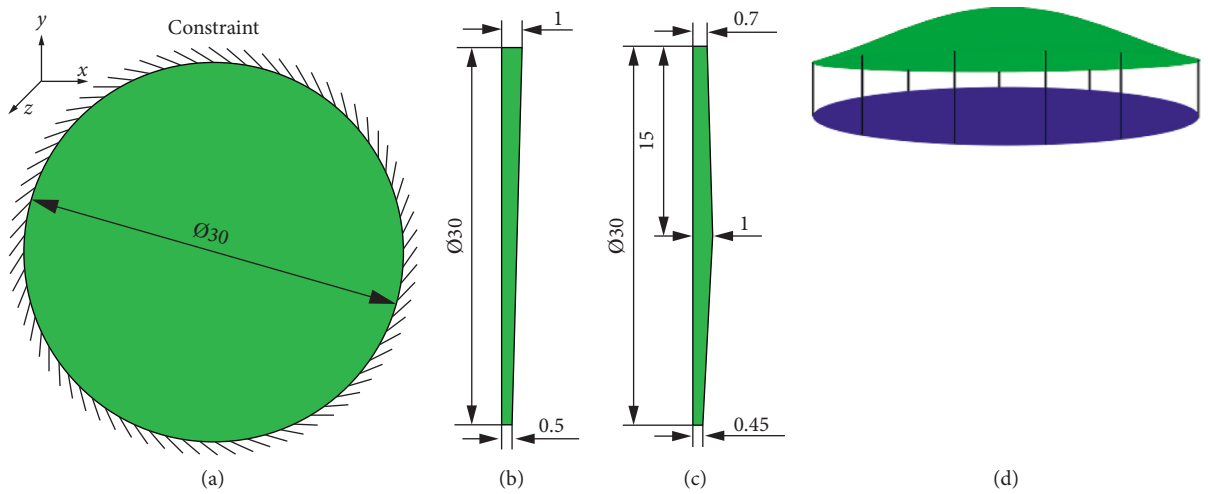


FIGURE 2: Model of geometry of the membrane. (a) Front view with constraint of full edge clamped. (b) Side view with one direction inclined membrane. (c) Side view with two directions inclined membrane. (d) Freeform surface structure with constraint of full edge clamped.

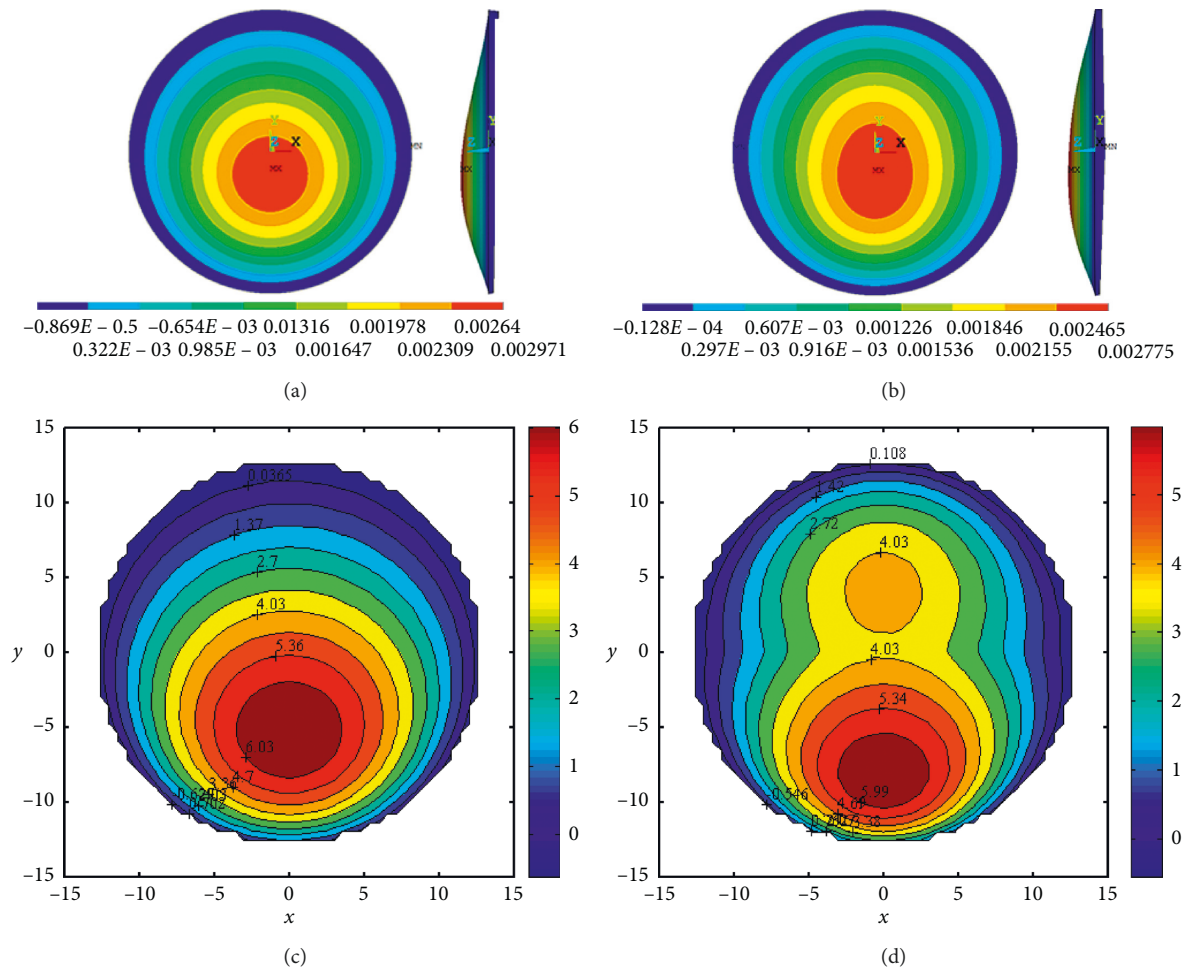


FIGURE 3: (a) The front view and left view of deformation displacement contour maps of one direction incline membrane under a pressure of 106 Pa. (b) The front view and left view of deformation displacement contour maps of two directions incline membrane under a pressure of 167 Pa. (c) The mean power distribution of one direction incline membrane under a pressure of 106 Pa. (d) The mean power distribution of two directions incline membrane under a pressure of 167 Pa.

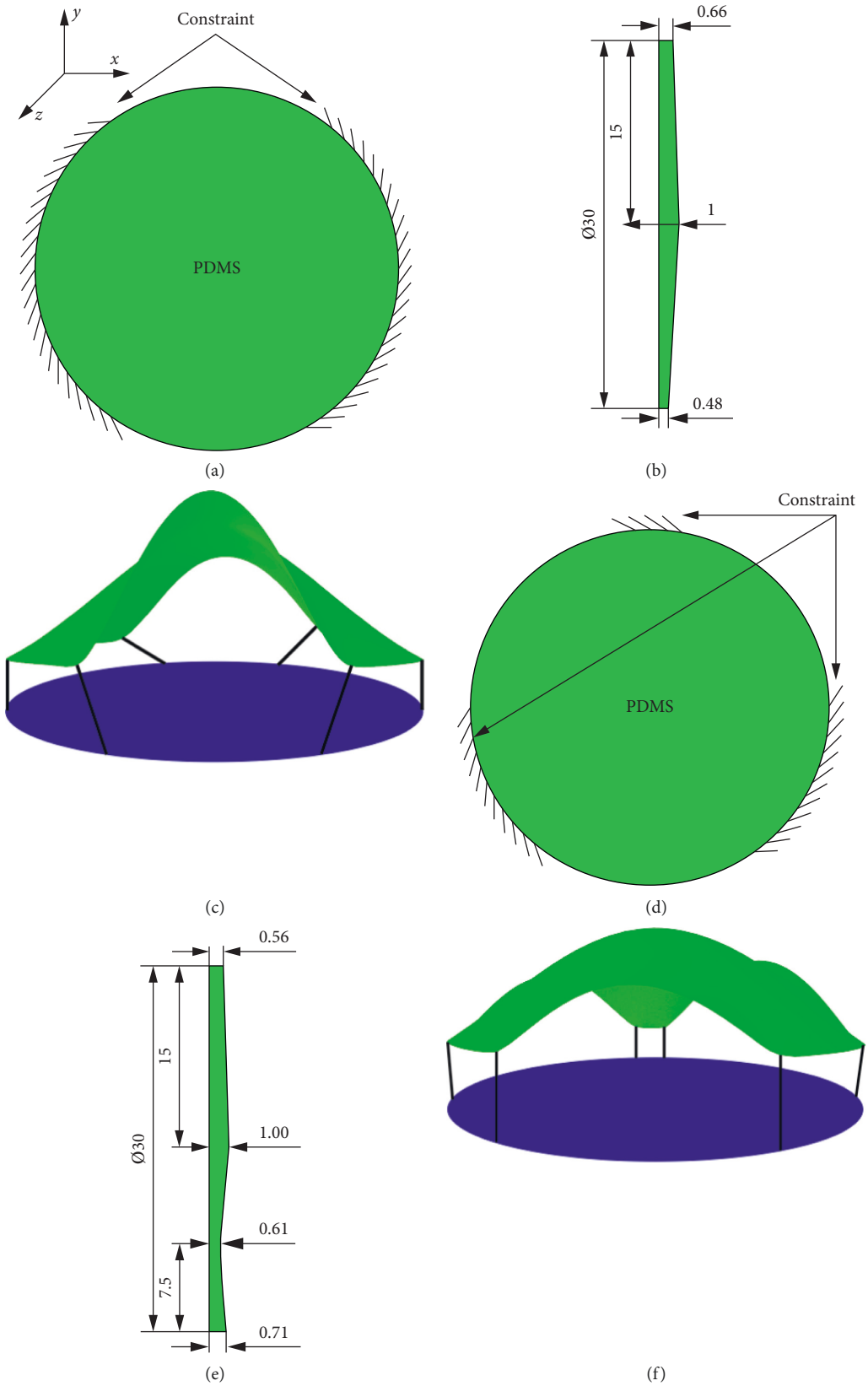


Figure 4: Model of geometry and surface structure of membranes. (a) Front view with constraint of two parts of edges clamped. (b) Side view with two directions inclined membrane. (c) Predicted freeform surface structure with constraint of two parts of edges clamped. (d) Front view with constraint of three parts of edges clamped. (e) Side view of a nonuniform thickness membrane. (f) Predicted freeform surface structure with constraint of three parts of edges clamped.

constraint of three parts of edge clamped and its front view and side view are shown in Figures 4(d) and 4(e). Based on the shape and constraints on the membranes, the corresponding freeform surface structures after deformation are predicted which are shown in Figures 4(c) and 4(f).

Then the 3D model files of two kinds of nonuniform thickness membranes are transferred to ANSYS software for meshing and simulation with different constraints under the pressure of 130 Pa and 104 Pa, and the deformation displacement contour maps of the front view and left view are shown in Figures 5(a) and 5(b). Then, the value of mean surface power of the two kinds of nonuniform thickness membranes can be calculated through the power distribution model, and the power value at the far view point and near view point of the two membranes are +4.07/+6.07 and +4.04/+6.00, which are illustrated in Figures 5(c) and 5(d). In conclusion, the optical power distribution characteristics of the far view region and near view region are similar under different constraints and pressure loads for the two kinds of nonuniform thickness membranes.

According to the simulation of the mean power distribution of three kinds of nonuniform thickness membranes with different constraints of full edge clamped, two parts of edges clamped and three parts of edges clamped are shown in Figures 3 and 5. Three kinds of liquid lenses based on the membranes can realize progressive multifocal; however, the scope of the far view region and near view region of the lens with a membrane of three parts of edges clamped is the largest, and the results are important inspiration to design a progressive multifocal liquid lens.

## 4. Tested Optical Characteristics

In order to evaluate the optical characteristics of fabricated liquid lenses, an optical experiment setup is constructed and the objective lens is used to take pictures which are observed onto a CMOS camera. The liquid lens is placed between the CMOS camera and F target, and the image of the F target can be observed clearly through adjusting the inner liquid pressure using a syringe pump and regulating the position of the lens along the guide rail.

The schematic diagram and a photograph of the optical experiment setup devised to check the focusing performance of the fabricated lens are shown in Figures 6 and 7, and the system consists of computer, vibration isolation table, guide rail, syringe pump, liquid lens, pressure gauge, F target, and CMOS camera. The CMOS camera is placed onto a precision guide rail, whose pixel size is $5.2 \times 5.2\,\mu$m, and the resolution of the CMOS sensor (DLC300-L) is $2048 \times 1563$ pixels. In the process of measurement, the distance between the end face position of the liquid lens and CMOS camera can be measured when the F target is observed focusing. In addition, a syringe pump is used to fine tune liquid pressure of the lens through pushing or pulling; then, the elastic membrane of the liquid lens is deformed, and the corresponding focal length will be altered.

The justification for the choice of different geometries is the characteristic of optical power distribution, especially for the liquid lens using nonuniform thickness membranes with different constraints to obtain $+4D/+6D$ in the far/near vision region. So, a prototype of an asymmetrical liquid lens is made according to the simulation results in Figure 3(d), and the aperture of the lens is 30 mm as shown in Figure 8, which include a mold, the front view, and side view of the lens before liquid injection. The lens is comprised of a nonuniform thickness PDMS membrane, a PMMA plate, pinhole, and the constraint of full edge clamped; therefore, the liquid-filled cavity of the lens is sealed with the nonuniform thickness PDMS membrane and PMMA plate. The adhesive ARseal 90880 (polypropylene double-sided adhesive tape) is used as the constraint to bond the PDMS membrane together with the PMMA plate. In this study, the circular ring of the adhesive film is used as the constraint to bond the PDMS membrane together with the PMMA plate. According to the shape of the membrane in Figures 2(a) and 2(c), the nonuniform thickness elastic membrane is made of polydimethylsiloxane (PDMS) SYLGARD 184 uncured mixture (10 : 1 ratio of base and curing agent) which was input into an aluminum alloy mold which is manufactured with ultraprecision machining and cured in an oven at 80°C for 40 minutes.

In the progressive addition liquid lens, the target surface profiles can be accurately replicated by the lens because the nonuniform thickness membranes are made from molds which are made according to the design and simulation, and the membranes will gain the desired shape with constraints through controlling the liquid pressure. The lens also can be optimized for best performance through adjusting the thickness distribution of the circular membrane and the type of constraints between the elastic membrane and support plate.

In the experiment, the liquid is injected by a syringe pump through a pinhole to deform the desired shape for the asymmetrical liquid lens under uniform liquid pressure which can be tuned through adjusting the flow rate or the moving speed of the pump. The diameter of the chamber is 30 mm, and the deformation characteristics of different regions of the lens are found to be different through the results of simulation. The original image of the F target before liquid injection is shown in Figure 9, and the focal length of the liquid lens can be measured through observing the F target is clear or not using a camera.

The liquid lens of the nonuniform thickness membrane with full edge clamped was made, and the representative images are shown in Figure 10 which were captured by the CMOS camera through the same liquid lens at different distances along the guide rail. Figure 10(a) shows the focused image located at the far view region of the lens, and the image is clear with focal length of $f = 310$ mm ($D = +3.22$) under a liquid pressure of 150 Pa, while the F target located at the near view region of the lens is blurred. Figure 10(b) shows the focused image located at the near view region of the lens, and the focal length is $f = 280$ mm ($D = +3.57$) under a liquid pressure of 150 Pa, while the image located at the far view region of the lens is blurred. Figure 10(c) shows that the image located at the far view region of the lens is focused, and the focal length is $f = 250$ mm ($D = +4.00$) under a liquid pressure of 167 Pa, while the image located at the near view

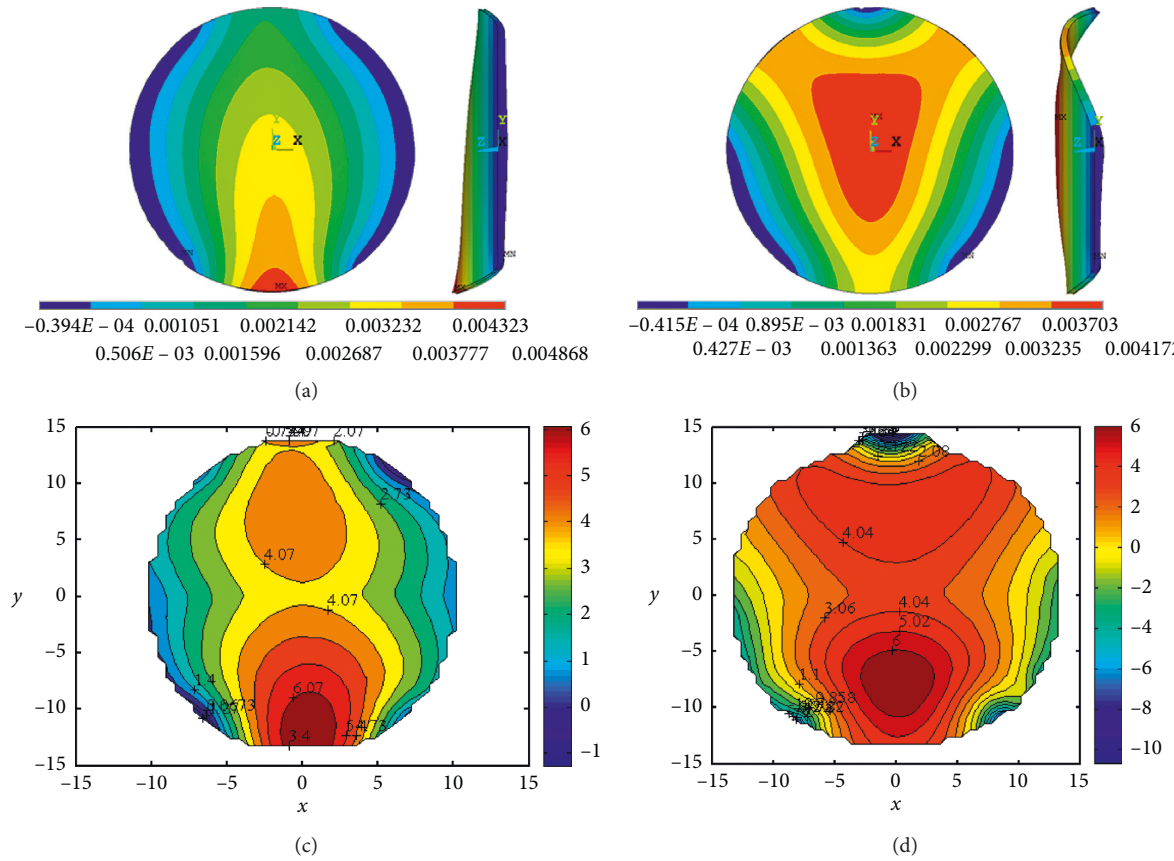


Figure 5: Deformation contour maps of front view and left view under pressures of (a) 130 Pa and (b) 104 Pa. Mean power distribution under different pressures of (c) 130 Pa and (d) 104 Pa.

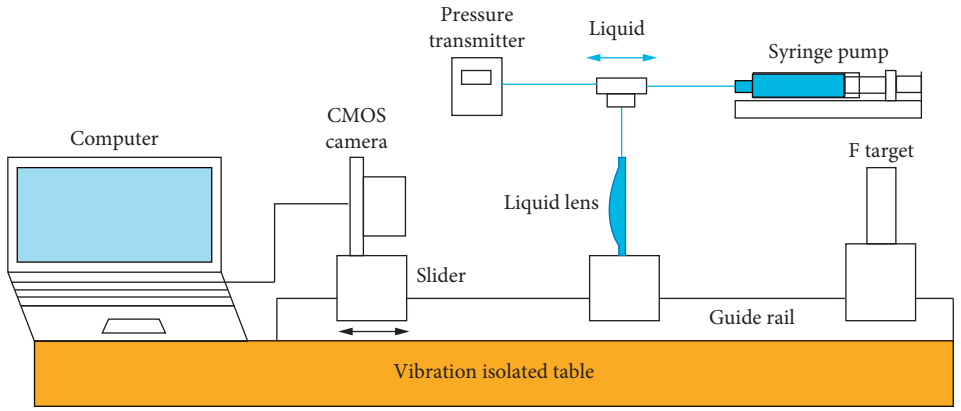


Figure 6: Schematic of the optical experiment setup used for image acquisition.

region of the lens is blurred. Figure 10(d) shows that the image located at the near view region of the lens is focused, and the focal length is $f = 220$ mm ($D = +4.54$) under the same liquid pressure, while the image located at the far view region of the lens is blurred.

Then, another two kinds of structure of asymmetrical multifocal liquid lens with different constraints are designed according to the simulation results in Figures 5(c) and 5(d). According to the shape of the nonuniform thickness PDMS membrane in Figures 4(a) and 4(b), the liquid lens with two parts of edges clamped was made and the liquid-filled cavity of the lens is sealed with a piece of uniform thickness The PDMS membrane and a piece of nonuniform thickness PDMS membrane are shown in Figures 11(a) and 11(b), which give the front view and top view of the lens after liquid injection into the cavity. In addition, two pieces of adhesive films located at the edge of the lens are used as the constraint to bond the PDMS membrane together with the PMMA

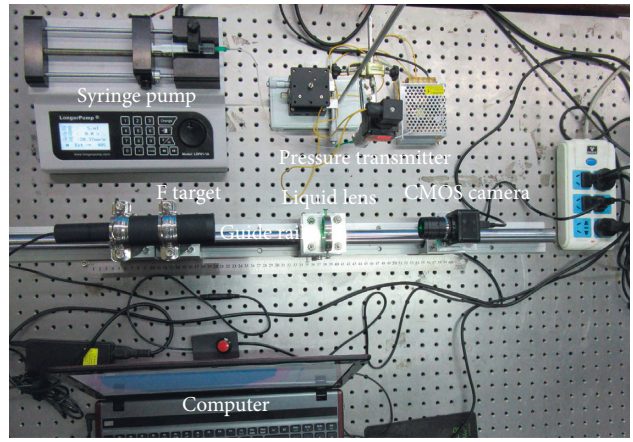


Figure 7: A photograph of the experimental setup to measure focusing performance of the fabricated lens.

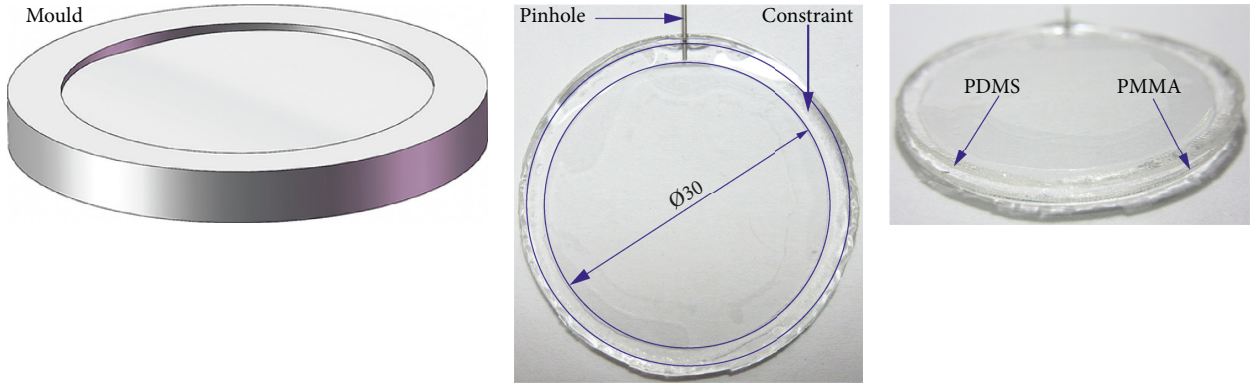


Figure 8: Liquid lens with the nonuniform thickness PDMS membrane. (a) Mold. (b) Front view. (c) Side view.

Figure 9: Original image of the F target before liquid injection.

plate. Then, according to the shape of the nonuniform thickness PDMS membrane in Figures 4(d) and 4(e), the liquid lens with three parts of edges clamped was made, and three pieces of adhesive films are used as the constraint to bond the PDMS membrane together with the PMMA plate which is shown in Figures 11(c) and 11(d), which give the front view and bottom view of the lens after liquid injection.

The representative images captured by a CMOS camera of the liquid lens with constraint of two parts of edge clamped are shown in Figures 12(a) and 12(b). Figure 12(a) shows that the focused image located at the far view region of the lens with the F target is clear, and the focal length is $f = 250$ mm ($D = +4.00$) under a liquid pressure of 130 Pa, while Figure 12(b) shows that the image located at the near view region of the lens is focused, and the focal length is $f = 200$ mm ($D = +5.00$) under the same liquid pressure. Plus, the representative images captured by a CMOS camera of the liquid lens with constraint of three parts of edge clamped are shown in Figures 12(c) and 12(d). Figure 12(c) shows that the focused image located at the far view region of the lens with the F target is clear, and the focal length is $f = 250$ mm ($D = +4.00$) under a liquid pressure of 104 Pa, while Figure 12(d) shows that the F target image located at the near view region of the lens is focused, and the focal length is $f = 170$ mm ($D = +5.88$) under the same liquid pressure.

The performances of the different structures of a liquid lens with a numerical aperture of 30 mm can be compared with each other through simulating the optical power

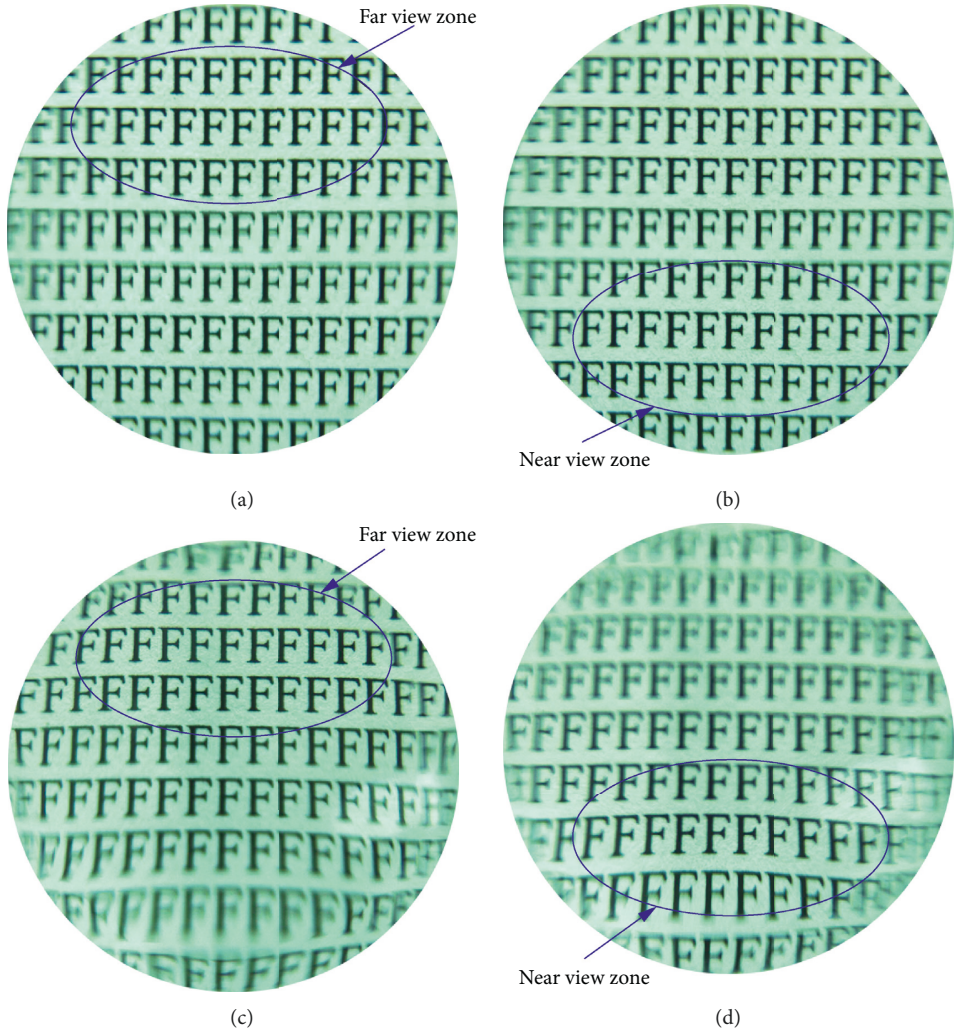


FIGURE 10: Test images of the F target for different focal lengths. (a) Focused image in the far view region ($f = 310$ mm). (b) Focused image in the near view region ($f = 280$ mm). (c) Focused image in the far view region ($f = 250$ mm). (d) Focused image in the near view region ($f = 220$ mm).

distribution and observing the focusing performance of the F target image in the experiment. Based on the results of the imaging tested experiment, liquid lenses with constraints of full edge clamped, two parts of edges clamped, and three parts of edges clamped were made as mentioned above, and they can realize as asymmetrical multifocal liquid lenses after liquid accommodation because one part of the image has good quality under certain liquid pressure and we can change the liquid pressure to obtain another part of the image which has good quality.

From the results of imaging tested experiment as shown in Table 1, imaging through the multifocal liquid lens with constraint of full edge clamped can obtain a focused image located at the far view region with $f = 310$ mm ($D = +3.22$) and focused image located at the near view region with $f = 280$ mm ($D = +3.57$) under a liquid pressure of 150 Pa, and also the lens can obtain a focused image located at the far view region with $f = 250$ mm ($D = +4.00$) and focused image located at the near view region with $f = 220$ mm ($D = +4.54$) under a liquid pressure of 167 Pa. In addition, the imaging through the liquid lens with constraint of two parts of edges clamped can obtain a focused image located at the far view region with $f = 250$ mm ($D = +4.00$) and focused image located at the near view region with $f = 200$ mm ($D = +5.00$) under a liquid pressure of 130 Pa. Furthermore, the F target image through the multifocal liquid lens with constraint of three parts of edges clamped can obtain a focused image located at the far view region with $f = 250$ mm ($D = +4.00$) and focused image located at the near view region with $f = 170$ mm ($D = +5.88$) under the liquid pressure of 104 Pa.

Three kinds of liquid lens of nonuniform thickness membranes with constraints of full edge clamped, two parts of edges clamped, and three parts of edges clamped are made. According to the experiment results of focusing performance, three kinds of liquid lens can realize progressive multifocal; however, the scope and the power value of the far view region and near view region of the lenses are different, and the scope of liquid lens with constraints of full edge clamped is larger; however, the optical power value of the power of liquid lens with constraints of three parts of

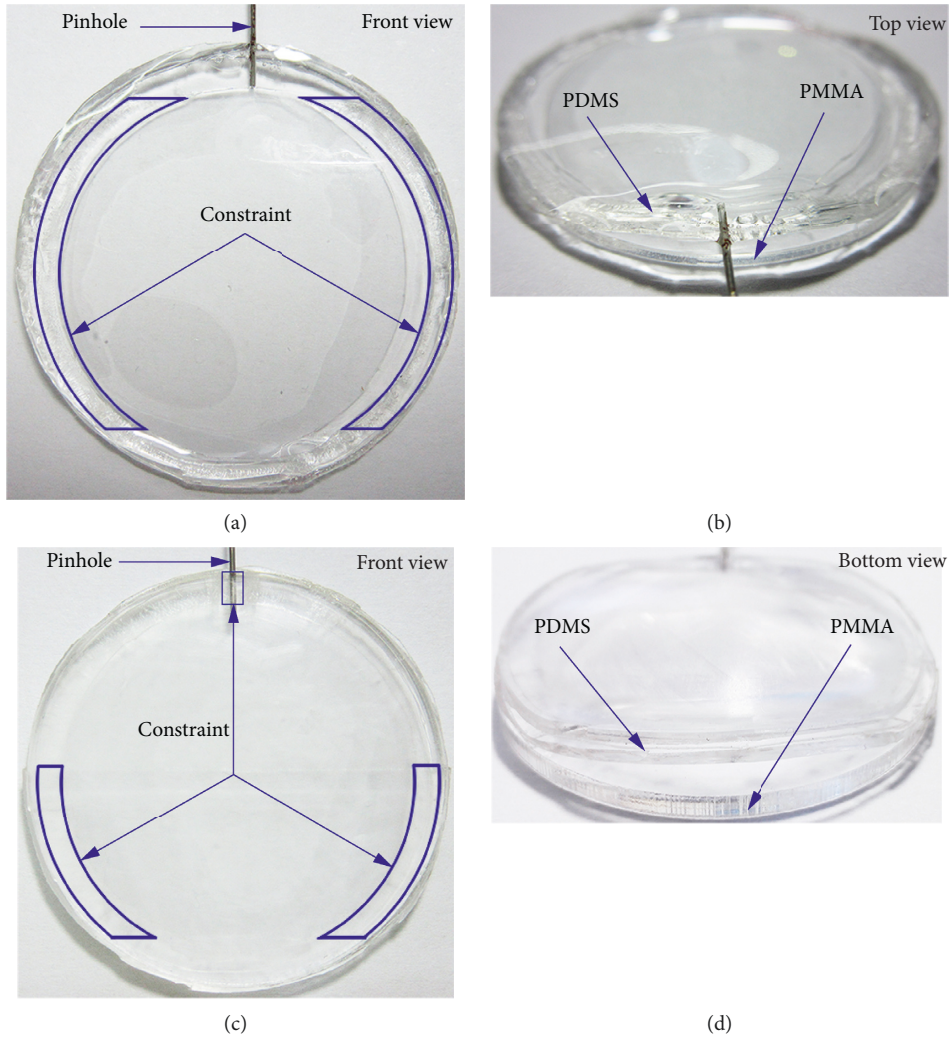


Figure 11: Liquid lens with constraint of two parts of edges clamped. (a) Front view. (b) Top view. Liquid lens with constraint of three parts of edges clamped. (c) Front view. (d) Bottom view.

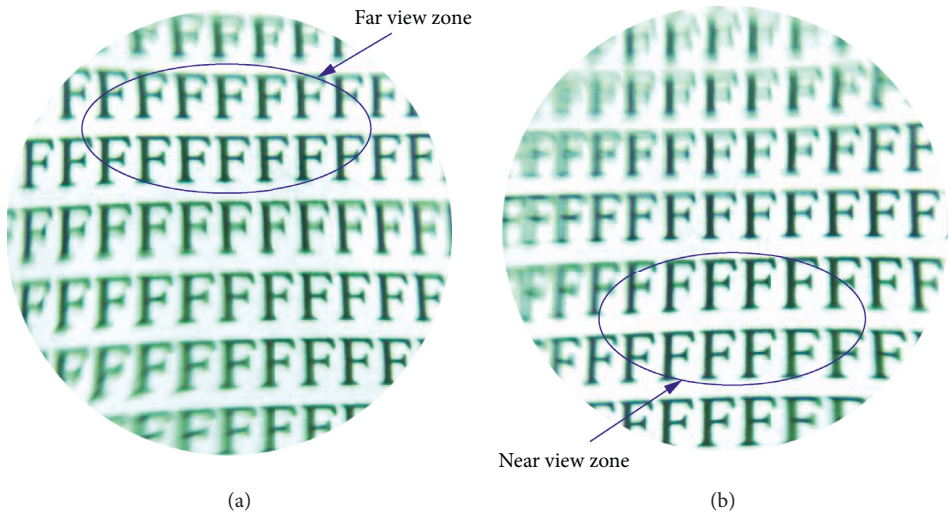


Figure 12: Continued.

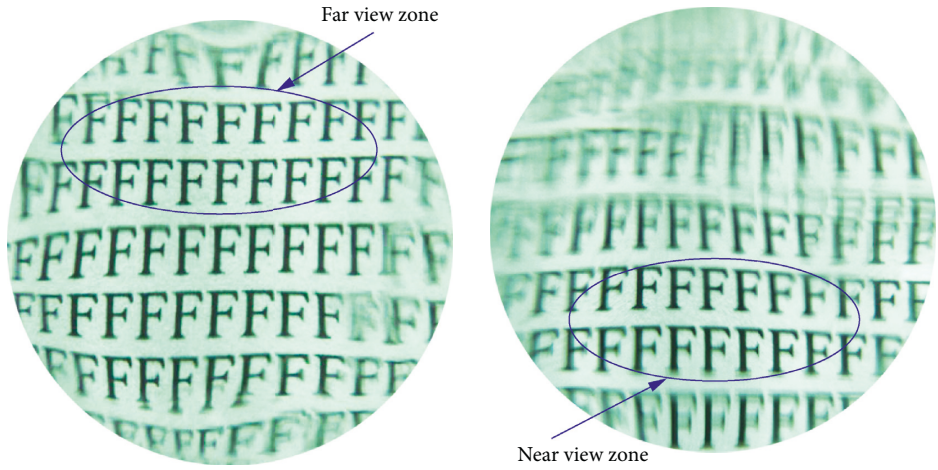


Figure 12: Test images of the F target for different focal lengths. (a) Focused image in the far view region ($f = 250$ mm). (b) Focused image in the near view region ($f = 200$ mm). (c) Focused image in the far view region ($f = 250$ mm). (d) Focused image in the near view region ($f = 170$ mm).

Table 1: The relationship of liquid pressure and focal length of three kinds of liquid lenses.

| Boundary conditions | Pressure (Pa) | Focal length (mm)/power | |
|---|---|---|---|
| | | Far view region | Near view region |
| Full edge constraint | 150 | 310 (+3.22) | 280 (+3.57) |
| | 167 | 250 (+4.00) | 220 (+4.54) |
| Two parts of edge constraint | 120 | 300 (+3.33) | 250 (+4.00) |
| | 130 | 250 (+4.00) | 200 (+5.00) |
| Three parts of edge constraint | 104 | 250 (+4.00) | 170 (+5.88) |
| | 130 | 200 (+5.00) | 150 (+6.67) |

edges clamped is closer to the simulation under the same pressure.

## 5. Conclusions

In this study, progressive multifocal liquid lenses are proposed which take advantage of nonuniform thickness PDMS membranes and PMMA plates with different constraint conditions. In the process of design, the thickness of the PDMS membrane can be designed nonuniform, and when a uniform pressure is applied onto the membrane, the deformation characteristics of the membrane with different constraints based on FEM simulations and corresponding power distribution can be obtained.

Based on the results of simulation, liquid lenses with constraints of full edge clamped, two parts of edge clamped, and three parts of edge clamped are designed and fabricated. Furthermore, the images of focusing performance of them are captured using an optical testing system. Experimental results demonstrate that they can realize as asymmetrical progressive multifocal liquid lenses after accommodation. The scope of liquid lens with constraints of full edge clamped is larger; however, the optical power value of the power of the liquid lens with constraints of three parts of edges clamped is closer to the simulation under the same pressure.

Although there are some deviations from the value of the experimental and simulation results, the reason may be that the thickness of membranes is not accurate enough in the experiment. The relationship between pressure onto the surface of the elastic membrane and the value of power can be obtained through the FEM simulation and power distribution model, and we can predict the value of optical power distribution (focal length) at different areas of the progressive multifocal liquid lens under different pressures. Then, more and better focusing performance of progressive multifocal liquid lenses can be designed with different thickness membranes and different constraints based on the results. The potential applications of the proposed progressive multifocal liquid lens could be in vision correction especially for presbyopia of old people at different environments and in the field of tunable optics.

## Data Availability

The data used to support the findings of this study are included within the article.

## Conflicts of Interest

The authors declare that they have no conflicts of interest.

## Authors' Contributions

Weiliang Jia carried out the lens structure design, simulation, and experiment analysis and wrote the paper. Biao Zhang helped the analysis with constructive discussions about the lens design and fabrication and provided a deeper insight into the related published work. Songjing Li built up the research project and was responsible in improving the quality of this paper.

## Acknowledgments

The authors would like to give their acknowledgement to the National Natural Science Foundation of China (no. 51175101) for the financial support to this study.

## References

[1] K. Wei, H. Huang, Q. Wang, and Y. Zhao, "Focus-tunable liquid lens with an aspherical membrane for improved central and peripheral resolutions at high diopters," *Optics Express*, vol. 24, no. 4, pp. 3929–3939, 2016.

[2] P. Pokorný, F. Šmejkal, P. Kulmon et al., "Calculation of nonlinearly deformed membrane shape of liquid lens caused by uniform pressure," *Applied Optics*, vol. 56, no. 21, pp. 5939–5947, 2017.

[3] D. Liang, D. T. Liang, X. Y. Wang, and P. Wang, "Flexible fluidic lens with polymer membrane and multi-flow structure," *Optics Communications*, vol. 421, pp. 7–13, 2018.

[4] A. Santiago-Alvarado, F. Iturbide-Jiménez, S. Vázquez-Montiel, and M. Ramírez Guzmán, "Optical design and analysis of a tunable focus liquid lens with meniscus surfaces," *Proceedings of SPIE*, vol. 7652, p. 76520W, 2010.

[5] D. Shaw and C.-W. Lin, "Design and analysis of an asymmetrical liquid-filled lens," *Optical Engineering*, vol. 46, no. 12, p. 123002, 2007.

[6] W.-C. Lin, C.-C. A. Chenb, and K.-C. Huang, "Design and fabrication of soft zoom lens," *Proceedings of SPIE*, vol. 7061, p. 70610W, 2008.

[7] A. Santiago-Alvarado, J. González-García, F. Itubide-Jiménez, M. Campos-García, V. M. Cruz-Martinez, and P. Rafferty, "Simulating the functioning of variable focus length liquid-filled lenses using the finite element method (FEM)," *Optik*, vol. 124, no. 11, pp. 1003–1010, 2013.

[8] D. Shaw and S. P. Cuo, "A study of the sensor shape of a hemispherical electronic eye variable focus camera lens," *Optical Review*, vol. 17, no. 6, pp. 541–548, 2010.

[9] S. T. Choi, B. S. Son, G. W. Seo, S.-Y. Park, and K.-S. Lee, "Opto-mechanical analysis of nonlinear elastomer membrane deformation under hydraulic pressure for variable-focus liquid-filled microlenses," *Optics Express*, vol. 22, no. 5, pp. 6133–6146, 2014.

[10] Y. Iimura, H. Onoe, T. Teshima, and Y. J. Heo, "Liquid-filled tunable lenticular lens," *Journal of Micromechanics and Microengineering*, vol. 25, p. 035030, 2015.

[11] C. Fang, B. Dai, R. Zhuo et al., "Focal-length-tunable elastomer-based liquid-filled plano-convex mini lens," *Optics Letters*, vol. 41, no. 2, pp. 404–407, 2016.

[12] A. Y. Malyuk and N. A. Ivanova, "Varifocal liquid lens actuated by laser-induced thermal Marangoni forces," *Applied Physics Letters*, vol. 112, no. 10, p. 103701, 2018.

[13] G. Lan, T. F. Mauger, and G. Li, "Design of high-performance adaptive objective lens with large optical depth scanning range for ultrabroad near infrared microscopic imaging," *Biomedical Optics Express*, vol. 6, no. 9, pp. 3362–3377, 2015.

[14] H.-M. Son, M. Y. Kim, and Y.-J. Lee, "Tunable-focus liquid lens system controlled by antagonistic winding-type SMA actuator," *Optics Express*, vol. 17, no. 16, pp. 14399–14350, 2009.

[15] N. Hasan, H. Kim, and C. H. Mastrangelo, "Large aperture tunable-focus liquid lens using shape memory alloy spring," *Optics Express*, vol. 24, no. 12, pp. 13334–13342, 2016.

[16] L. Wang, H. Oku, and M. Ishikawa, "Variable-focus lens with 30 mm optical aperture based on liquid-membrane-liquid structure," *Applied Physics Letters*, vol. 102, no. 13, p. 131111, 2013.

[17] L. Wang, H. Oku, and M. Ishikawa, "An improved low-optical-power variable focus lens with a large aperture," *Optics Express*, vol. 22, no. 16, pp. 19448–19456, 2014.

[18] P. Zhao, Ç. Ataman, and H. Zappe, "Gravity-immune liquid-filled tunable lens with reduced spherical aberration," *Applied Optics*, vol. 55, no. 28, pp. 7816–7823, 2016.

[19] P. Zhao, Ç. Ataman, and H. Zappe, "An endoscopic microscope with liquid-tunable aspheric lenses for continuous zoom capability," *Proceedings of SPIE*, vol. 9130, p. 913004, 2014.

[20] P. Zhao, Ç. Ataman, and H. Zappe, "Spherical aberration free liquid-filled tunable lens with variable thickness membrane," *Optics Express*, vol. 23, no. 16, pp. 21264–21278, 2015.

[21] H. Huang, W. Kang, Q. Wang, and Y. Zhao, "Improved optical resolution for elastomer-liquid lens at high dioptre using varied thickness membrane," *Proceedings of SPIE*, vol. 9705, p. 970504, 2016.

[22] M. C. Flores-Bustamante, M. Rosete-Aguilar, and S. Calixto, "Mechanical and optical behavior of a tunable liquid lens using a variable cross section membrane: modeling results," *Proceedings of SPIE*, vol. 9699, p. 969908, 2016.

[23] Z. Ding, C. Wang, Z. Hu et al., "Surface profiling of an aspherical liquid lens with a varied thickness membrane," *Optics Express*, vol. 25, no. 4, pp. 3122–3132, 2017.

[24] M. Shimoda and K. Yamane, "A numerical form-finding method for the minimal surface of membrane structures," *Structural and Multidisciplinary Optimization*, vol. 51, no. 2, pp. 333–345, 2015.

[25] L. Wang, Q. Zhang, and B. Yang, "Free form design for single layer shell structures," in *Proceedings of the 2010 IEEE International Conference on Progress in Informatics and Computing*, pp. 1062–1066, Shanghai, China, December 2010.

[26] J. Strasky, P. Juchelková, P. Kaláb, and R. Nečas, "Roofs of prestressed concrete membranes," *Structural Concrete*, vol. 18, no. 1, pp. 5–18, 2017.

[27] T. Steele, H. McLoughlin, and D. Payne, "Progressive addition power lenses," U.S. Patent 6776486 B2, 2004.

[28] Z. Li and D. Li, "Surface analysis and evaluation of progressive addition lens," *Proceedings of SPIE*, vol. 10154, p. 101540M, 2016.

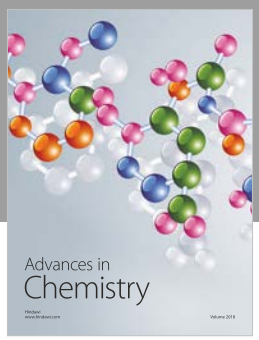

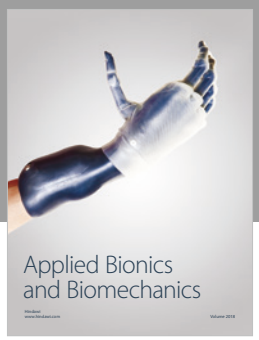

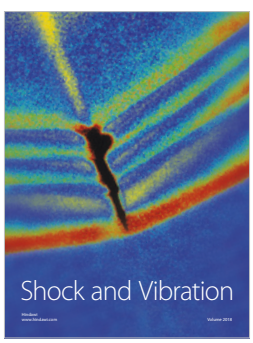

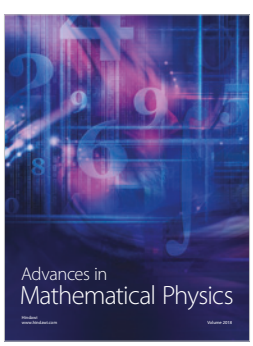

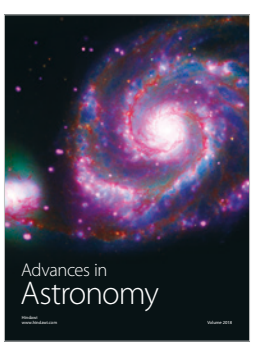

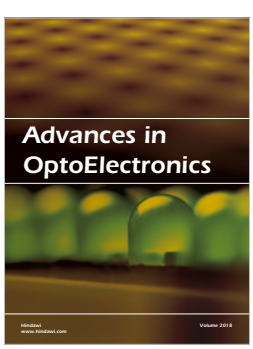

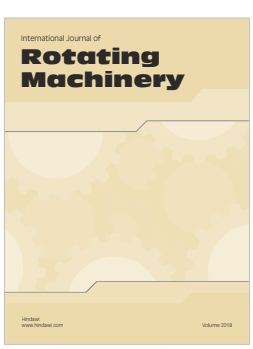

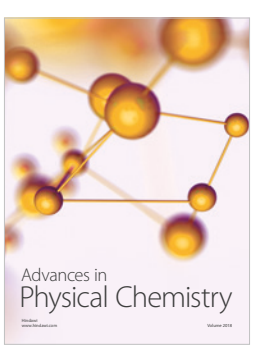

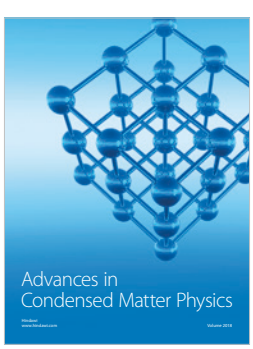

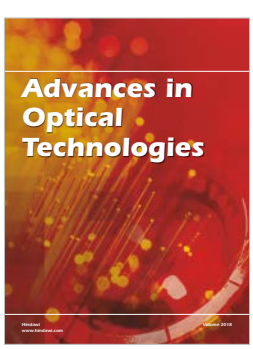

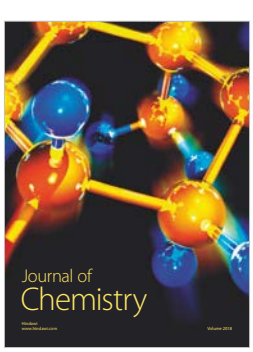

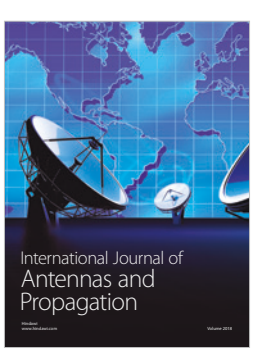

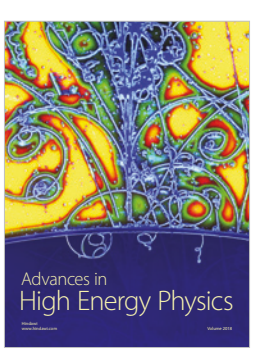

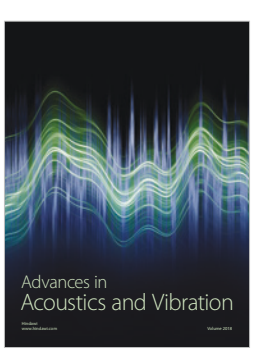

Hindawi

Submit your manuscripts at
www.hindawi.com